Generation of classical non-Gaussian states by squeezing a thermal state into nonlinear motion of levitated optomechanics

R. Muffato , ^{1,2} T. S. Georgescu, ¹ J. Homans , ¹ T. Guerreiro , ² Q. Wu, ³ D. A. Chisholm, ³ M. Carlesso , ^{4,5,3} M. Paternostro , ^{6,3} and H. Ulbricht , ^{1,*}

¹School of Physics and Astronomy, University of Southampton, Southampton SO17 1BJ, United Kingdom

²Department of Physics, Pontifical Catholic University of Rio de Janeiro, Rio de Janeiro, Brazil

³Centre for Quantum Materials and Technologies, School of Mathematics and Physics, Queen's University Belfast,

Belfast BT7 1NN, United Kingdom

⁴Department of Physics, University of Trieste, Strada Costiera 11, 34151 Trieste, Italy
⁵Istituto Nazionale di Fisica Nucleare, Trieste Section, Via Valerio 2, 34127 Trieste, Italy
⁶Dipartimento di Fisica e Chimica - Emilio Segrè, Università degli Studi di Palermo, via Archirafi 36, I-90123 Palermo, Italy

(Received 10 January 2024; accepted 6 January 2025; published 18 February 2025)

We report on an experiment achieving the dynamical generation of non-Gaussian states of motion of a levitated optomechanical system. We access intrinsic Duffing-like nonlinearities by thermal squeezing of an oscillator's state of motion by rapidly switching the frequency of its trap. We characterize the experimental non-Gaussian state versus expectations from simulations and give prospects for the emergence of genuine nonclassical features.

DOI: 10.1103/PhysRevResearch.7.013171

I. INTRODUCTION

Macroscopic quantum states are regarded as ideal platforms to test the existence of intrinsic limitations in quantum formalism [1] and the effects of gravity in quantum systems [2]. While various platforms have been considered for generating such states [3], levitated systems have emerged as a front-runner in light of the possibility to achieve remarkable environmental isolation [4] and embed control techniques in their dynamics. Engineering nonclassical states of levitated mechanical systems is achieved by inducing nonlinear dynamics to sufficiently coherent initial states of motion [5,6]. Accessing nonlinearity by motional squeezing-sometimes assisted by a dark trap-can be instrumental to preparing nonclassical states [7]. The fundamental building block of such operations, namely, the squeezing of thermal states of motion of levitated particles, has been demonstrated by rapid (i.e., faster than the oscillation frequency) switching between different trap frequencies [8], as theoretically proposed by Janszky and Yushin [9], or using cavities [10,11]. Such switches can be treated as pulses applied to the particle's spring constant and have been used to drive a classical harmonic oscillator [12]. Repeated gentle squeezing pulses applied to the thermal motional state's momentum can increase the particle's oscillation amplitude, allowing it to explore the nonlinear flat extremities of the trapping potential while remaining trapped. Correspondingly, the dynamics can pick up Duffing-like nonlinearities, as already demonstrated

Published by the American Physical Society under the terms of the Creative Commons Attribution 4.0 International license. Further distribution of this work must maintain attribution to the author(s) and the published article's title, journal citation, and DOI.

[13]. This scheme dynamically shapes the potential landscape, creating bistability. Classical effects have been discussed before in relation to fields such as memory elements [14], signal amplification via stochastic resonance [15], nonequilibrium physics [16], nonlinear dynamics, synchronization [17], and active escape dynamics [18]. It is also predicted to enhance force sensing capabilities of levitated mechanics [19].

In this paper, we experimentally demonstrate how a sequence of repeated pulses can be used to dynamically produce a significantly non-Gaussian state of motion by accessing intrinsic trapping-potential nonlinearities and controlling their effects. We show the time trace, in phase space, of the motional state resulting from the application of our protocol to an initial thermal state, demonstrating the emergence of nontrivial transient bimodal distributions whose relaxation dynamics we characterize experimentally. Moreover, we provide a quantitative perspective for the emergence of genuine quantum features of motion from a sufficiently coherent initial state of the particle [20–24]. We show how this would result in negative phase-space distributions, thus unambiguously demonstrating nonclassicality, a key feature for quantum information processing and fundamental tests of quantum mechanics.

II. THEORETICAL MODEL

We refer to the setting illustrated in Fig. 1(a), which depicts a nanoparticle trapped in an optical tweezer in vacuum. In general, the particle motion occurs in all three spatial directions (x, y, z), including cross coupling between orthogonal directions of motion [17] and possibly involving rotational motion as well. However, our analysis focuses only on the x motion. We model the stochastically driven and damped oscillatory motion of a levitated particle in a vacuum using a one-dimensional Langevin-type equation for the time-dependent position x(t) of the center-of-mass motion of

^{*}Contact author: H.Ulbricht@soton.ac.uk

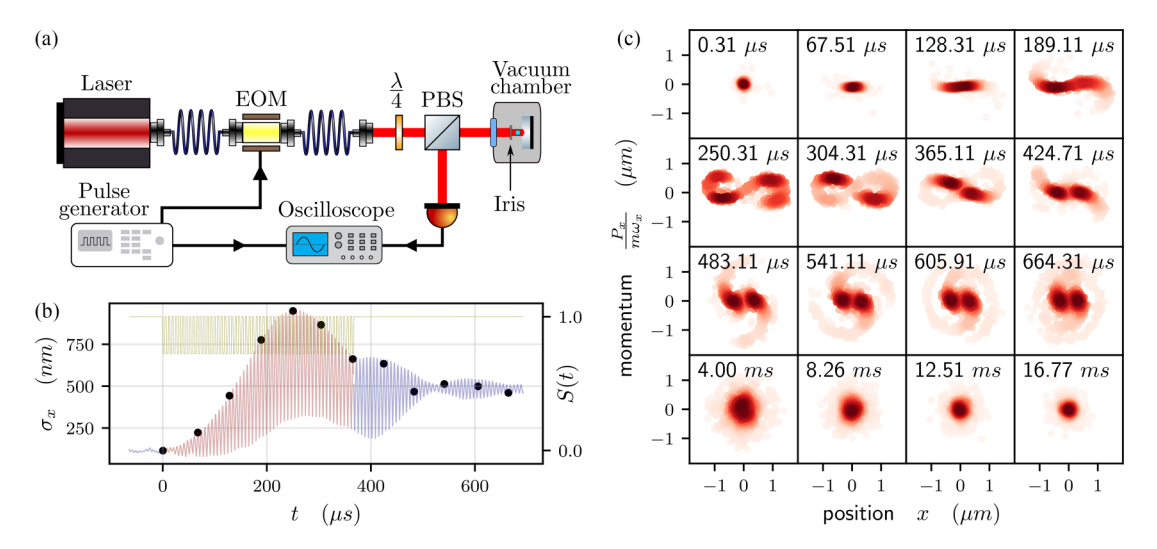


FIG. 1. (a) Schematic of the experimental setup. A silica nanoparticle is trapped by optical tweezers in vacuum. An electro-optical modulator (EOM) controlled by a pulse generator modulates the power of the laser. The oscilloscope receives the signal from the particle. Its acquisition is triggered by a synchronous signal from a pulse generator. (b) Experimental time evolution of the standard deviation of the particle position as measured by the photodiode (blue and red line). The green line is the intensity modulation function S(t) [see Eq. (1)] applied to the trapping laser beam via the EOM. (c) Experimental time trace of the phase-space distribution of an initial thermal state of motion of the particle subjected to our protocol. The first 12 snapshots of the distribution are indicated as black dots in (b). The last line depicts the thermalization occurring at a longer timescale.

a particle of mass m in the trap,

$$\ddot{x}(t) = -\Gamma_m \dot{x}(t) + S(t) \frac{F(x)}{m} + \frac{\mathcal{F}_{\text{fluct}}(t)}{m}, \tag{1}$$

where, in the regime dominated by the background gas pressure P, the damping rate can be written as [25]

$$\Gamma_m = \frac{64r^2P}{m\overline{v}_{\rm gas}},\tag{2}$$

with \overline{v}_{gas} being the root-mean-square thermal velocity of the gas molecules at room temperature and r and m being the radius and mass of the trapped silica particle. The second term on the right-hand side of Eq. (1) is the position-dependent restoring force originating from the interaction with a Gaussian light beam in the Rayleigh regime. In the large oscillation-amplitude limit, when the nonlinearity becomes effective, this force is given by

$$F(x) = \frac{2\pi n_m r^3}{c} \left(\frac{n_r^2 - 1}{n_\pi^2 + 2}\right) \frac{\partial I}{\partial x},\tag{3}$$

with n_m and n_p being the refractive indices of the medium and of the silica particle (here assumed to take the nominal values of 1 and 1.44, respectively), $n_r = n_p/n_m$ being the relative refractive index, c being the speed of light, and I being the intensity of the trapping laser beam. Equation (3) gives rise to a nonlinear force directed along the gradient of the optical potential U(x) such that $F(x) = -\partial_x U(x)$ [26–28], which we control by modulating in time the power of the trapping laser according to the function S(t) in Eq. (1) and as illustrated in Fig. 1(b) [8]. The last term on the right-hand side of Eq. (1) describes the driving of the harmonic motion by random background gas collisions, which are modeled as the timedependent stochastic force $\mathcal{F}_{\text{fluct}}(t) = \sqrt{2\Gamma_m k_B T} \eta(t)$. Here, k_B is Boltzmann's constant, and T is the temperature of the gas surrounding the oscillating particle [29], while $\eta(t)$ is a zero-mean, δ -correlated Gaussian white noise such that $\langle \eta(t)\eta(t')\rangle = \delta(t-t')$. We have integrated Eq. (1) numerically using the Euler-Maruyama method [30] and by sampling the initial values of the position and momentum of the particle from a thermal state. The results of our analysis are shown as phase-space probability distributions in Figs. 2(a)–2(c), which show that our one-dimensional description of the dynamics is sufficient to produce the main features of experimental data.

III. EXPERIMENT

The experimental setup is illustrated in Fig. 1(a). We use a parabolic mirror to focus light at a wavelength of 1550 nm to a diffraction-limited spot of the diameter of 1 µm. A pulse generator (Berkeley BNC 525) and an electro-optical modulator (EOM, Jenoptik AM1550b) are used to modulate the laser intensity as a square wave with high and low levels of 80 and 57 mW, respectively, to trap a silica particle with a close to spherical shape (460 nm diameter) from a spray in the focal point. We monitor the center-of-mass motion of the trapped particle by detecting a small fraction of Rayleigh backscattered light from the trapping field with a single photodiode detector (see Ref. [31] for technical details). An iris is mounted on top of the parabola to suppress unwanted light reflected from the flat edges of the mirror and make sure that all the detected signal comes from only the particle. This guarantees the reliable assessment of the particle's center-of-mass position with only negligible distortions by the bandpass filtering process, as analyzed in more detail in Sec. A of the Supplemental Material (SM) [32]. Calibration of motional amplitudes and the mass of the trapped particle was done assuming perfect equilibrium of the particle with the background gas at 5 mbar by fitting a Lorentzian to the trap frequency peak, see Supplemental Material for details [31,32].

To prepare bimodal states of motion the pressure is further reduced to $1 \times 10^{-2} \, \text{mbar}$, and the particle resonance

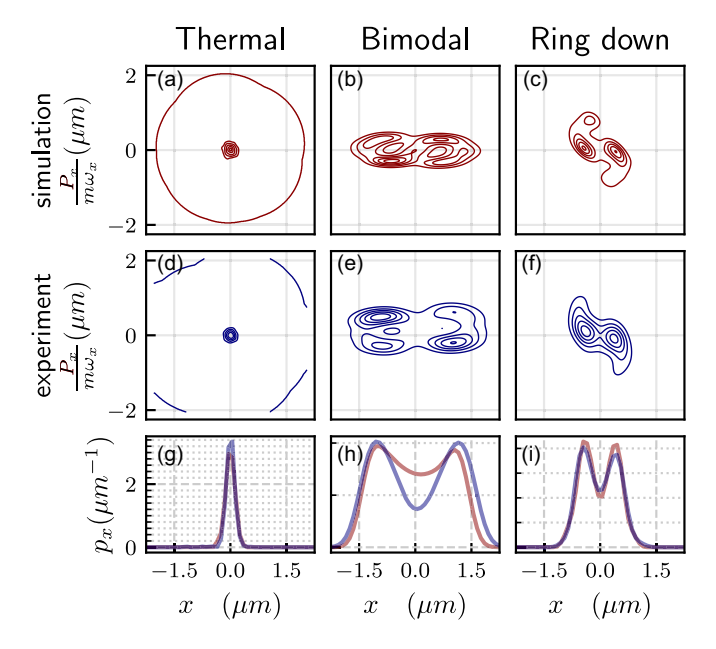


FIG. 2. Comparisons between simulations (red lines) and experimental reconstructions (blue lines) of the phase-space distributions associated with paradigmatic states of motion of the levitated particle. (a) and (d) Initial thermal state. (b) and (e) Initial non-Gaussian bimodal state. (c) and (f) The initial distribution is that of the motional state achieved by stopping the dynamical protocol. Such a state will eventually relax back to a thermal configuration. (g)–(i) show the projection of the phase-space distribution, with p_x being the position probability function for the three initial states described above.

frequency $\omega/2\pi = 77 \, kHz$ is evaluated from the spectrum of the signal at the high-power level. Next, thermal squeezing is achieved by modulating the scale of the restoring force term of Eq. (1) as S(t), with

$$S(t) = \begin{cases} 1 & \text{for } t' = 0 \text{ or } t' \in [\tau_{\text{low}}, \tau_{\text{low}} + \tau_{\text{high}}], \\ 0.71 & \text{for } t' \in [0, \tau_{\text{low}}]. \end{cases}$$
(4)

Here, $t' = t \mod (\tau_{\text{low}} + \tau_{\text{high}})$. Each pulse is timed so that the particle completes a quarter of an oscillation at the highpower level, $\tau_{\text{high}} = \pi/2\omega = 3.25 \,\mu\text{s}$, and another quarter of an oscillation at the low-power level, $\tau_{\text{low}} = \pi/2\omega\sqrt{S} =$ $3.48\,\mu s$. The duration at the low-power level is slightly longer due to the rescaling of dynamics by the relative decrease of power. One pulse sequence consists of a train of 55 pulses as constructed on the pulse generator to prepare the bimodal state. Data acquisition by the oscilloscope is synchronized with the pulse generator, and 689 pulse sequences are acquired, with 518 ms between successive sequences, which is about 25 times longer than the extracted 20 ms relaxation time, in good agreement with Eq. (2), allowing the particle to relax back to the thermal state between consecutive runs, see Supplemental Material Sec. G for details [32]. We experimentally characterize a Duffing nonlinearity $\xi = -0.1 \, \mu \text{m}^{-2}$ for our parabolic mirror trapping potential, $U(x) = \omega^2 x^2 +$ $w^2 \xi x^4$, as described in more detail in Ref. [13]. See Supplemental Material for more details [32].

IV. RESULTS AND DISCUSSION

The trap nonlinearity generating the non-Gaussian state is small under typical experimental conditions [25]. Taylor expansion of the gradient force up to third order shows that the inverse of the Duffing parameter is proportional to the square of the beam's waist. Considering it to be a measure for the range of nonlinearity, we note that it is larger than the spread of the thermal state $\sigma_{\text{thermal}} = \sqrt{k_B T/k}$, where k is the optomechanical spring constant and T is the motional temperature. This means that the particle hardly visits the nonlinear part of the potential. By squashing the motional state, we induce sufficient elongation such that the vertexes of the state are eventually extended to nonlinear parts of the potential well and the nonlinear effect dominates the dynamics. In these regions, the particle's dynamics is slower due to a softer effective spring constant making the tip of the ellipse lag behind compared to the faster harmonic behavior near the center. In the course of sufficiently many weak pulses, the state changes its shape, steadily transforming it from the initial circular thermal Gaussian to a squashed ellipsoidal and eventually to a curved spiral in which probability mass starts to accumulate, forming a multimodal state. We emphasize that in general, for very large motions self-homodyne detection might become substantially nonlinear, potentially affecting the phase-space distributions. Possible ways to avoid these effects are to cool the motion to ensure the homodyne detection stays linear [14] and to benchmark homodyne detection against heterodyne measurements to rule out nonlinearities in the detection [33].

To quantify the non-Gaussianity of the resulting simulated and experimentally obtained states, we adopt a nondimensional measure of bimodality [34],

$$A_D = \frac{\sqrt{2}}{\sigma_r} |\mu_1 - \mu_2|,\tag{5}$$

where $\mu_{1,2}$ are the positions of the peaks of the distribution and $\sigma_T = \sqrt{\sum_{i=1}^2 \sigma_i^2}$ is defined in terms of the individual peak's variances $\sigma_{1,2}$ [see Fig. 2(h)]. By curve fitting a double Gaussian function to our experimental and simulated data we find the values $A_D^{\text{exp}} = 3.95$ and $A_D^{\text{sim}} = 3.32$, in good agreement with 12% deviation, which we identify to originate from a small difference in the shape of the real trapping potential compared with the simulated one. The influence of the potential's nonlinearity is understood to be negligible in the linear section near the trap center and to become dominant towards the asymptotically flat edges of the optical trap. Despite us knowing the general features of the nonlinearity of the potential well, its exact profile is not experimentally known. As such, simulations assuming an ideal sharp beam profile were found to deviate more from the experimental results. We also find that the experimental thermal state has some outlier points that overextend the tails of Gaussian distribution, which are not included in the simulations and contribute to a softening of the potential and a larger value for A_D^{exp} . We explain outliers as a buildup of amplitude as a net effect of multiple collisions by background gas particles or other perturbations affecting the trap. See Supplemental Material for details [32].

V. PERSPECTIVES FOR QUANTUM EXPERIMENT

To investigate nonlinear squeezing effects provided by the protocol for a quantum system, we consider the system Hamiltonian

$$\hat{H}_s(t) = \frac{\hat{p}_x^2}{2m} - S(t)U_0 e^{-2\hat{x}^2/w_0^2},\tag{6}$$

where \hat{x} and \hat{p}_x are the position and momentum operators. The potential of the system, represented by the second term, is an inverted Gaussian like that used in the classical simulation, with its gradient corresponding to Eq. (3). Here, U_0 sets the energy scale (the depth) of the potential, and S(t) is the control given by Eq. (4). We assume that the experiment is performed in a low-pressure, cryogenic environment, such that it is possible to perform scattering-free experiment runs [35]. In this regime, the dynamics of the system follows the von Neumann master equation, $\hat{\rho}(t) = -\frac{i}{\hbar}[\hat{H}_s(t), \hat{\rho}(t)] - \Lambda[\hat{x}, [\hat{x}, \hat{\rho}]]$, where the second term describes the decoherence due to photon recoils [36].

For a typical optolevitating experiment, the size of the quantum system is way smaller than that of the trapping potential. Therefore, the challenge of this quantum experiment is to expand the quantum system to the spread (FWHM) of the potential approximated by the focus beam waist w_0 before complete decoherence, so that systems like the one reported above can exhibit nonclassical features such as negativity in the Wigner distribution N(t). The negativity N(t) is defined by integrating the Wigner distribution over the region of the phase space Σ_- , where it attains negative values, that is,

$$N(t) = \iint_{\Sigma} dx dp_x W_{x,p_x}(t).$$
 (7)

For a highly focused Gaussian beam, the beam waist can be reduced to $\omega_0 \approx 750$ nm (the Duffing parameter $\xi \approx -0.3~\mu\text{m}^{-2}$). We assume that the quantum system can be expanded by a factor of $\zeta=100$ through a fast squeezing protocol [36]. This means that we need to prepare an initial quantum system of size $\Delta x_0 \approx 7.5$ nm. This is difficult, as the zero-point fluctuation of the motion is approximately $\Delta x_{zpf} = \sqrt{\hbar/2m\omega} = 0.01$ nm for a nanoparticle of R=50 nm ($\rho=2200~\text{kg/m}^3$) trapped at frequency $\omega/2\pi=50$ kHz. Indeed, this bottlenecks all the schemes to prepare large mass non-classical states—the mismatch between the scale of the beam trap and the coherence length of a massive quantum system.

One way to approach this issue is to consider a smaller nanoparticle and prepare the *n*th Fock state as the initial state. Indeed, a smaller particle yields a smaller decoherence rate and a larger quantum state. Consider a nanoparticle of R=4 nm trapped at frequency $\omega/2\pi=80$ kHz. The decoherence constant Λ depends on the particle size (and other experimental details), and we estimate it with the equation [37,38]

$$\Lambda = \frac{7\pi\,\varepsilon_0}{30\hbar} \left(\frac{\epsilon_c V E_0}{2\pi}\right)^2 k_0^5,\tag{8}$$

where ε_0 is the vacuum permittivity and $\epsilon_c = 3(\epsilon-1)/(\epsilon+2)$, with ϵ being the relative dielectric constant of the nanoparticle. V is the volume of the nanoparticle, $k_0 = 2\pi/\lambda$, and $E_0 = \sqrt{4P_0/\pi\varepsilon_0}\,c\,w_0^2A_xA_y$, where P_0 is the tweezer power, w_0 is the beam waist, A_x and A_y are the

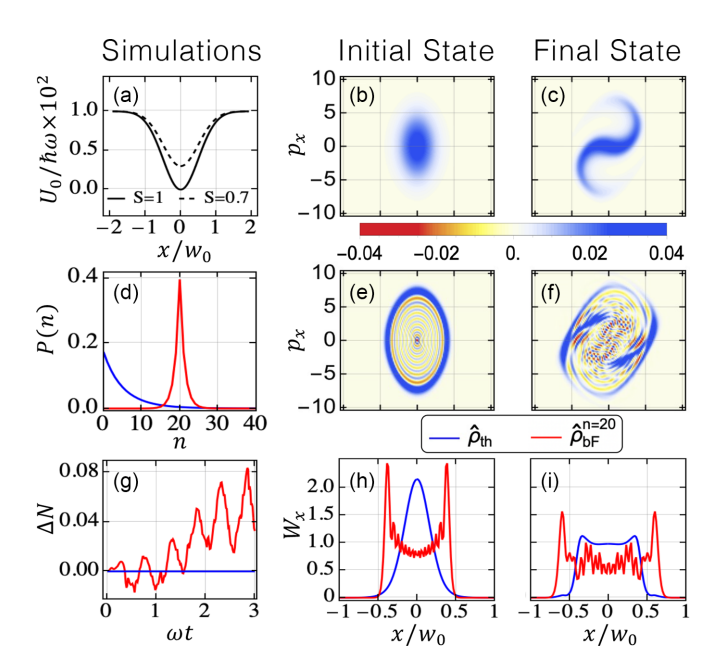


FIG. 3. Simulations of the nonlinear protocol for quantum systems. (a) shows the oscillating potentials with $U_0/\hbar\omega=100$ energy levels. (b) and (e) are the Wigner distribution for the initial thermal state $\hat{\rho}_{\rm th}$ and the initial blurred Fock state $\hat{\rho}_{\rm bF}^{n=20}$, and (c) and (f) are those of the final state at $\omega t=11/4$. (d) shows the population distributions P(n) for the initial states. (g) shows the increment of negative Wigner distribution ΔN over three oscillations. (h) and (i) show the marginal Wigner distribution W_x of the initial and final systems. Here, the blue line represents the thermal state $\hat{\rho}_{\rm th}$, and the red line represents the blurred Fock state $\hat{\rho}_{\rm bE}^{n=20}$.

asymmetry factors, and c is the speed of light. Taking the values in Ref. [39], the decoherence constant Λ is estimated to be $\Lambda \approx 3.28 \times 10^{19} \ \mathrm{Hz} \ \mathrm{m}^{-2}$. The corresponding decoherence rate $\Gamma = \Lambda \Delta x_{zpf}^2 \approx 5.8 \ \mathrm{Hz}$, such that $\Gamma/\omega \approx 1.16 \times 10^{-5}$. On the other hand, the nth Fock state has the standard position variance $\Delta x^n = \sqrt{(2n+1)\hbar/2m\omega}$, such that $\Delta x^{100} \approx 6$ nm for the state $|n=100\rangle$. Based on the estimation in Sec. G in the SM [32], the initial system $|n=100\rangle$ can be expanded by a factor of $\zeta=100$ and can reach $\Delta x_{\mathrm{expanded}}^{100} \approx 600$ nm, with remaining system purity $\mathcal{P} \approx 0.9$.

We performed simulations with a smaller quantum system to demonstrate the effects of the protocol (details are reported in Sec. H in the SM [32]) and show the results in Fig. 3. The system considered here has $U_0/\hbar\omega = 100$ energy levels in the potential, as shown by Fig. 3(a). We take two kinds of initial states with roughly the same energy, the thermal state $\hat{\rho}_{th}$ [40] and the blurred Fock state $\hat{\rho}_{bF}^{n=20}$ [which is the Gaussian mixture centered at the Fock state $|n = 20\rangle$, defined by Eq. (S11) in the SM [32]], as an example of the aforementioned quantum experiment. Their population distributions P(n) are shown in Fig. 3(d), and their Wigner distributions are shown by Figs. 3(b) and 3(e). We simulate the nonlinear protocol with these two initial states for oscillation time $\omega t = 11/4$ and decoherence rate $\Gamma/\omega = 10^{-5}$ and show the Wigner distributions for the final states in Figs. 3(c) and 3(f). The marginal Wigner distributions W_x for the initial and final states are shown by Figs. 3(h) and 3(i), and the increment of the Wigner negativity $\Delta N = N(t) - N(0)$ is recorded in Fig. 3(g).

From the outcomes, we draw the following conclusions. First, taking the thermal state $\hat{\rho}_{th}$ as the initial state, we retrieve a behavior similar to that in the classical experiment (Gaussian to bimodal distribution), although it works at a much lower energy. However, due to the mixture of the Fock states, we observe no increment of negative Wigner distribution when taking this initial state.

Second, taking the mixed Fock state $\hat{\rho}_{bF}^{n=20}$ as the initial state (see Sec. I in the SM for other initial states [32]), we still see the nonlinear effect of the protocol (in terms of the increasing separation of two peaks in the marginal Wigner distribution) as well as the increment of the Wigner negativity. This protocol shows the potential of generating non-Gaussian states with nonclassical features [Figs. 3(g)-3(i)] by coherently expanding the initial quantum state enough to access the nonlinearity of the potential.

However, generating such Fock states at current experimental conditions is challenging. The requirements can be potentially relaxed in a more sophisticated experiment. Introducing extrinsic nonlinearity [41] can reduce the requirement for the expansion rate ζ by enhancing the Duffing parameter ξ . For example, actuating the system, either externally [42] or parametrically, conditioned on real-time position measurement, has the potential to modify the effective dynamics. Another measure is reducing the photon recoil rate Γ by taking a zero-information measurement [43], with implementation ideas for levitated systems [44,45]. Such improvements could potentially facilitate the initiation of this protocol from a low-energy thermal state, enabling the generation of a bimodal distribution while likely preserving quantum coherence.

Finally, we note that optomechanical state tomography was successfully demonstrated in the classical regime for clamped [46] and levitated [47] systems, with several proposals extending the technique to the quantum regime [48–50], including approaches utilizing neural networks [51]. However, a specific quantum procedure to extract Wigner negativity for levitated optomechanics systems has yet to be fully developed and requires further research.

VI. CONCLUSION

We showed experimentally that controlled access of intrinsic trap nonlinearities can be used for the generation of non-Gaussian classical states. We showed theoretically that, if the motional state is initially prepared as a Fock state, using the fast squeezing protocol allows the system to access the intrinsic trap nonlinearities with high remaining purity. Experimental improvements can be realized to achieve non-Gaussian states on smaller length scales, thus diminishing decoherence effects, for instance, using stronger nonlinearities, such as those from engineered potentials [6], and deploying quantum control methods of thermodynamic inspiration [52], which will be the focus of forthcoming work. Then, our scheme can be used to generate bimodal states with a genuinely nonclassical character, as witnessed by significantly negative Wigner distributions. We note the experimental realization of a very similar protocol for squeezing in the nonlinear mechanical quantum system in the gigahertz regime with the result of negativity [53]. Periodically driving mechanical motion as in our squeezing protocol is also predicted to enhance force sensing capabilities of levitated mechanics [19].

ACKNOWLEDGMENTS

We thank J. Wardak, E. Simcox, and C. Timberlake for discussions. We acknowledge funding from the EPSRC International Quantum Technologies Network Grant Levinet (EP/W02683X/1). We further acknowledge financial support from the U.K. funding agency EPSRC (Grants No. EP/W007444/1, No. EP/V035975/1, No. EP/V000624/1, No. EP/X009491/1, and No. EP/T028424/1), the Leverhulme Trust (RPG-2022-57 and RPG-2018-266), the Royal Society Wolfson Fellowship (RSWF/R3/183013), the Department for the Economy Northern Ireland under the US-Ireland R&D Partnership Programme, the EU Horizon 2020 FET-Open project TeQ (766900), the PNRR PE Italian National Quantum Science and Technology Institute (PE0000023), and the EU Horizon Europe EIC Pathfinder project QuCoM (Grant Agreement No. 10032223). We further acknowledge support from the QuantERA grant LEMAQUME, funded by the QuantERA II ERA-NET Cofund in Quantum Technologies implemented within the EU Horizon 2020 Program.

DATA AVAILABILITY

Data are available from the University of Southampton Institutional Repository [54].

M. Arndt and K. Hornberger, Testing the limits of quantum mechanical superpositions, Nat. Phys. 10, 271 (2014).

^[2] D. Carney, P. C. Stamp, and J. M. Taylor, Tabletop experiments for quantum gravity: A user's manual, Classical Quantum Gravity **36**, 034001 (2019).

^[3] S. Nimmrichter and K. Hornberger, Macroscopicity of mechanical quantum superposition states, Phys. Rev. Lett. 110, 160403 (2013).

^[4] C. Gonzalez-Ballestero, M. Aspelmeyer, L. Novotny, R. Quidant, and O. Romero-Isart, Levitodynamics: Levitation

and control of microscopic objects in vacuum, Science 374, eabg3027 (2021).

^[5] M. Roda-Llordes, A. Riera-Campeny, D. Candoli, P. T. Grochowski, and O. Romero-Isart, Macroscopic quantum superpositions via dynamics in a wide double-well potential, Phys. Rev. Lett. 132, 023601 (2024).

^[6] A. A. Rakhubovsky, D. W. Moore, and R. Filip, Nonclassical states of levitated macroscopic objects beyond the ground state, Quantum Sci. Technol. 4, 024006 (2019).

^[7] E. Bonvin, L. Devaud, M. Rossi, A. Militaru, L. Dania, D. S. Bykov, O. Romero-Isart, T. E. Northup, L. Novotny, and M.

- Frimmer, State expansion of a levitated nanoparticle in a dark harmonic potential, Phys. Rev. Lett. **132**, 253602 (2024).
- [8] M. Rashid, T. Tufarelli, J. Bateman, J. Vovrosh, D. Hempston, M. S. Kim, and H. Ulbricht, Experimental realization of a thermal squeezed state of levitated optomechanics, Phys. Rev. Lett. 117, 273601 (2016).
- [9] J. Janszky and Y. Y. Yushin, Squeezing via frequency jump, Opt. Commun. 59, 151 (1986).
- [10] T. W. Penny, A. Pontin, and P. F. Barker, Sympathetic cooling and squeezing of two colevitated nanoparticles, Phys. Rev. Res. 5, 013070 (2023).
- [11] Y. Li, A.-N. Xu, L.-G. Huang, and Y.-C. Liu, Mechanical squeezing via detuning-switched driving, Phys. Rev. A 107, 033508 (2023).
- [12] V. I. Arnol'd, Mathematical Methods of Classical Mechanics (Springer New York, NY, 2013).
- [13] A. Setter, J. Vovrosh, and H. Ulbricht, Characterization of non-linearities through mechanical squeezing in levitated optomechanics, Appl. Phys. Lett. 115, 153106 (2019).
- [14] M. Frimmer, T. L. Heugel, Ž. Nosan, F. Tebbenjohanns, D. Hälg, A. Akin, C. L. Degen, L. Novotny, R. Chitra, O. Zilberberg *et al.*, Rapid flipping of parametric phase states, Phys. Rev. Lett. 123, 254102 (2019).
- [15] F. Ricci, R. A. Rica, M. Spasenović, J. Gieseler, L. Rondin, L. Novotny, and R. Quidant, Optically levitated nanoparticle as a model system for stochastic bistable dynamics, Nat. Commun. 8, 15141 (2017).
- [16] J. Gieseler, R. Quidant, C. Dellago, and L. Novotny, Dynamic relaxation of a levitated nanoparticle from a non-equilibrium steady state, Nat. Nanotechnol. 9, 358 (2014).
- [17] J. Gieseler, M. Spasenović, L. Novotny, and R. Quidant, Non-linear mode coupling and synchronization of a vacuum-trapped nanoparticle, Phys. Rev. Lett. **112**, 103603 (2014).
- [18] A. Militaru, M. Innerbichler, M. Frimmer, F. Tebbenjohanns, L. Novotny, and C. Dellago, Escape dynamics of active particles in multistable potentials, Nat. Commun. 12, 2446 (2021).
- [19] F. Cosco, J. S. Pedernales, and M. B. Plenio, Enhanced force sensitivity and entanglement in periodically driven optomechanics, Phys. Rev. A 103, L061501 (2021).
- [20] F. Tebbenjohanns, M. L. Mattana, M. Rossi, M. Frimmer, and L. Novotny, Quantum control of a nanoparticle optically levitated in cryogenic free space, Nature (London) 595, 378 (2021).
- [21] U. Delić, M. Reisenbauer, K. Dare, D. Grass, V. Vuletić, N. Kiesel, and M. Aspelmeyer, Cooling of a levitated nanoparticle to the motional quantum ground state, Science 367, 892 (2020).
- [22] L. Magrini, P. Rosenzweig, C. Bach, A. Deutschmann-Olek, S. G. Hofer, S. Hong, N. Kiesel, A. Kugi, and M. Aspelmeyer, Real-time optimal quantum control of mechanical motion at room temperature, Nature (London) 595, 373 (2021).
- [23] M. Kamba, R. Shimizu, and K. Aikawa, Optical cold damping of neutral nanoparticles near the ground state in an optical lattice, Opt. Express 30, 26716 (2022).
- [24] A. Ranfagni, K. Børkje, F. Marino, and F. Marin, Two-dimensional quantum motion of a levitated nanosphere, Phys. Rev. Res. 4, 033051 (2022).
- [25] J. Gieseler, L. Novotny, and R. Quidant, Thermal nonlinearities in a nanomechanical oscillator, Nat. Phys. 9, 806 (2013).
- [26] P. H. Jones, O. M. Maragò, and G. Volpe, *Optical Tweezers: Principles and Applications* (Cambridge University Press, Cambridge, 2015).

- [27] A. Ashkin, J. M. Dziedzic, J. E. Bjorkholm, and S. Chu, Observation of a single-beam gradient force optical trap for dielectric particles, Opt. Lett. 11, 288 (1986).
- [28] Y. Harada and T. Asakura, Radiation forces on a dielectric sphere in the rayleigh scattering regime, Opt. Commun. 124, 529 (1996).
- [29] R. Kubo, The fluctuation-dissipation theorem, Rep. Prog. Phys. 29, 255 (1966).
- [30] G. Volpe and G. Volpe, Simulation of a Brownian particle in an optical trap, Am. J. Phys. 81, 224 (2013).
- [31] J. Vovrosh, M. Rashid, D. Hempston, J. Bateman, M. Paternostro, and H. Ulbricht, Parametric feedback cooling of levitated optomechanics in a parabolic mirror trap, J. Opt. Soc. Am. B 34, 1421 (2017).
- [32] See Supplemental Material at http://link.aps.org/supplemental/ 10.1103/PhysRevResearch.7.013171 for more experimental and theoretical details.
- [33] C. Dawson and J. Bateman, Spectral analysis and parameter estimation in levitated optomechanics, J. Opt. Soc. Am. B 36, 1565 (2019).
- [34] K. M. Ashman, C. M. Bird, and S. E. Zepf, Detecting bimodality in astronomical datasets, Astron. J. **108**, 2348 (1994).
- [35] D. S. Bykov, P. Mestres, L. Dania, L. Schmöger, and T. E. Northup, Direct loading of nanoparticles under high vacuum into a Paul trap for levitodynamical experiments, Appl. Phys. Lett. 115, 034101 (2019).
- [36] T. Weiss, M. Roda-Llordes, E. Torrontegui, M. Aspelmeyer, and O. Romero-Isart, Large quantum delocalization of a levitated nanoparticle using optimal control: Applications for force sensing and entangling via weak forces, Phys. Rev. Lett. 127, 023601 (2021).
- [37] C. Gonzalez-Ballestero, P. Maurer, D. Windey, L. Novotny, R. Reimann, and O. Romero-Isart, Theory for cavity cooling of levitated nanoparticles via coherent scattering: Master equation approach, Phys. Rev. A 100, 013805 (2019).
- [38] T. Seberson and F. Robicheaux, Distribution of laser shot-noise energy delivered to a levitated nanoparticle, Phys. Rev. A **102**, 033505 (2020).
- [39] We take the particle radius R=4 nm, the laser wavelength $\lambda=1550$ nm, the laser power $P_0=0.5$ W, the trap width $w_0=750$ nm, the vacuum permittivity $\varepsilon_0=8.9\times 10^{-21}$ F/nm, the relative dielectric constant $\epsilon=2$, and the asymmetry factors $A_x=1$ and $A_y=0.9$.
- [40] We take mean excitation number $\langle n \rangle = (\exp[\hbar\omega/k_BT] 1)^{-1} = 4.52$. Here, ω is the oscillation frequency approximated in the low-energy section of our inverted Gaussian system (e.g., in our example $\omega/2\pi = 80$ kHz). The variance of this thermal state is half of that of the blurred Fock state, as shown by Fig. 3(h).
- [41] D. Hempston, J. Vovrosh, M. Toroš, G. Winstone, M. Rashid, and H. Ulbricht, Force sensing with an optically levitated charged nanoparticle, Appl. Phys. Lett. 111, 133111 (2017).
- [42] O. Kremer, D. Tandeitnik, R. Mufato, I. Califrer, B. Calderoni, F. Calliari, B. Melo, G. Temporão, and T. Guerreiro, Perturbative nonlinear feedback forces for optical levitation experiments, Phys. Rev. A 109, 023521 (2024).
- [43] S. S. Szigeti, A. R. R. Carvalho, J. G. Morley, and M. R. Hush, Ignorance is bliss: General and robust cancellation of decoherence via no-knowledge quantum feedback, Phys. Rev. Lett. 113, 020407 (2014).

- [44] R. Gajewski and J. Bateman, Backaction suppression in levitated optomechanics using reflective boundaries, arXiv:2405.04366.
- [45] Y. Weiser, T. Faorlin, L. Panzl, T. Lafenthaler, L. Dania, D. S. Bykov, T. Monz, R. Blatt, and G. Cerchiari, Back action suppression for levitated dipolar scatterers, Phys. Rev. A 111, 013503 (2025).
- [46] M. Vanner, J. Hofer, G. Cole, and M. Aspelmeyer, Cooling-by-measurement and mechanical state tomography via pulsed optomechanics, Nat. Commun. 4, 2295 (2013).
- [47] M. Rashid, M. Toroš, and H. Ulbricht, Wigner function reconstruction in levitated optomechanics, Quantum Meas. Quantum Metrol. 4, 17 (2017).
- [48] M. R. Vanner, I. Pikovski, and M. Kim, Towards optomechanical quantum state reconstruction of mechanical motion, Ann. Phys. (Berlin, Ger.) 527, 15 (2015).
- [49] F. Shahandeh and M. Ringbauer, Optomechanical state reconstruction and nonclassicality verification beyond the resolved-sideband regime, Quantum 3, 125 (2019).

- [50] P. Warszawski, A. Szorkovszky, W. P. Bowen, and A. C. Doherty, Tomography of an optomechanical oscillator via parametrically amplified position measurement, New J. Phys. 21, 023020 (2019).
- [51] T. Weiss and O. Romero-Isart, Quantum motional state tomography with nonquadratic potentials and neural networks, Phys. Rev. Res. 1, 033157 (2019).
- [52] Q. Wu, M. A. Ciampini, M. Paternostro, and M. Carlesso, Quantifying protocol efficiency: A thermodynamic figure of merit for classical and quantum state-transfer protocols, Phys. Rev. Res. 5, 023117 (2023).
- [53] S. Marti, U. von Lüpke, O. Joshi, Y. Yang, M. Bild, A. Omahen, Y. Chu, and M. Fadel, Quantum squeezing in a nonlinear mechanical oscillator, Nat. Phys. 20, 1448 (2024).
- [54] T. S. Georgescu, R. Mufato Reis, and H. Ulbricht, Data for: Generation of classical non-Gaussian states by squeezing a thermal state into nonlinear motion of levitated optomechanics, University of Southampton, 2025, https://doi.org/10.5258/ SOTON/D3337.